IJMMM International Journal of Minerals, Metallurgy and Materials 矿物冶金与材料学报（英文版）

Review of precipitation strengthening in ultrahigh-strength martensitic steel

Zhihao Tian, Chunlei Shang, Chaolei Zhang, Xiaoye Zhou, Honghui Wu, Shuize Wang, Guilin Wu, Junheng Gao, Jiaming Zhu, and Xinping Mao

Cite this article as:
Zhihao Tian, Chunlei Shang, Chaolei Zhang, Xiaoye Zhou, Honghui Wu, Shuize Wang, Guilin Wu, Junheng Gao, Jiaming Zhu, and Xinping Mao, Review of precipitation strengthening in ultrahigh-strength martensitic steel, *Int. J. Miner. Metall. Mater.*, 32(2025), No. 2, pp. 256-269. https://doi.org/10.1007/s12613-024-2994-5

View the article online at SpringerLink or IJMMM Webpage.

INTERNATIONAL JOURNAL OF
Minerals, Metallurgy and Materials

Volume 32, Number 2, February 2025
Page 256

Review

https://doi.org/10.1007/s12613-024-2994-5

Review of precipitation strengthening in ultrahigh-strength martensitic steel

Zhihao Tian[1),*], *Chunlei Shang*[1),*], *Chaolei Zhang*[1,2),✉], *Xiaoye Zhou*[3)], *Honghui Wu*[1,2,4),✉], *Shuize Wang*[1,2)], *Guilin Wu*[1,2)], *Junheng Gao*[1,2)], *Jiaming Zhu*[5)], *and Xinping Mao*[1,2)]

1) Institute for Carbon Neutrality, University of Science and Technology Beijing, Beijing 100083, China
2) Institute of Steel Sustainable Technology, Liaoning Academy of Materials, Shenyang 110004, China
3) Department of Materials Science and Engineering, Shenzhen MSU-BIT University, Shenzhen 518172, China
4) Institute of Materials Intelligent Technology, Liaoning Academy of Materials, Shenyang 110004, China
5) School of Civil Engineering, Shandong University, Jinan 250061, China
(Received: 3 May 2024; revised: 20 August 2024; accepted: 21 August 2024)

Abstract: Martensite is an important microstructure in ultrahigh-strength steels, and enhancing the strength of martensitic steels often involves the introduction of precipitated phases within the martensitic matrix. Despite considerable research efforts devoted to this area, a systematic summary of these advancements is lacking. This review focuses on the precipitates prevalent in ultrahigh-strength martensitic steel, primarily carbides (e.g., MC, M_2C, and M_3C) and intermetallic compounds (e.g., NiAl, Ni_3X, and Fe_2Mo). The precipitation-strengthening effect of these precipitates on ultrahigh-strength martensitic steel is discussed from the aspects of heat treatment processes, microstructure of precipitate-strengthened martensite matrix, and mechanical performance. Finally, a perspective on the development of precipitation-strengthened martensitic steel is presented to contribute to the advancement of ultrahigh-strength martensitic steel. This review highlights significant findings, ongoing challenges, and opportunities in the development of ultrahigh-strength martensitic steel.

Keywords: ultrahigh-strength martensitic steel; precipitation strengthening; mechanical property; carbide; intermetallic compound

1. Introduction

Martensite is a critical microstructure, and the martensitic matrix is the foundation of ultrahigh-strength steels (UHSSs) [1]. Enhanced martensitic steel strength is frequently achieved through the incorporation of nanoprecipitates, such as ultrahigh-strength (UHS) maraging steel [2–9] and secondary hardening steel [10–17], to reinforce the matrix. Owing to its excellent mechanical properties, UHS maraging steel is widely used in many important fields, such as aerospace, power plants, and maritime construction [18–23]. The nanoprecipitates within UHS maraging steel, including the dispersed fine carbides and the intermetallic compounds formed through alloying and subsequent precipitation during heat treatment, obstruct dislocation movement and thereby significantly enhance the steel's strength [24]. Despite these advancements, a comprehensive overview of the precipitates responsible for precipitation strengthening in UHS martensitic steel is lacking.

For UHS martensitic steel, carbides such as MC, M_2C, and M_3C are usually introduced for precipitation strengthening. For example, Dong *et al.* [25] used transmission electron microscopy (TEM) and X-ray diffraction (XRD) to characterize the microstructure and precipitates of Nb–V–Ti microalloyed UHS steel. Their study revealed that M_3C precipitated during tempering at 200–400°C and was partially replaced by M_2C and $M_{23}C_6$ when the temperature was raised to 500°C. When the temperature was above 600°C, M_3C disappeared, and part of M_2C transformed into M_7C_3. Li *et al.* [26] utilized scanning electron microscopy (SEM), optical microscopy (OM), XRD, and TEM to study the precipitates and mechanical properties and the effect of carbide distribution on the mechanical properties of AF1410 steel. The results showed three kinds of carbides present in the steel, namely, spherical MC, $M_{23}C_6$ carbides, and short rod-shaped M_2C carbides. Furthermore, excessive tempering temperature can result in the coarsening of carbides, leading to a decrease in ultimate tensile strength (UTS) and yield strength. Mondiere *et al.* [27] comprehensively analyzed the microstructure using XRD, TEM, and correlative atom probe tomography (APT) to investigate the precipitation of different carbides in Ferrium M54. Ti-rich MC carbides precipitate at high temperatures. Intensive and efficient nanoscale M_2C carbides precipitate during tempering, resulting in a UTS of 1965 MPa. Despite many investigations into the mechanisms of carbide for precipitation strengthening in UHS martensitic steel, a systematic summary is lacking.

Intermetallic compounds, including NiAl, Ni_3Ti, Ni_3Mo,

*These authors contributed equally to this work.

✉ Corresponding authors: Chaolei Zhang E-mail: zhangchaolei@ustb.edu.cn; Honghui Wu E-mail: wuhonghui@ustb.edu.cn

Springer

and Fe_2Mo, are also key precipitates that enhance precipitation strengthening in UHS martensitic steel. To reduce the cost of UHS martensitic steel while maintaining high strength, Nong *et al.* [28] developed an innovative Co/Mo-free maraging steel wherein the nanoscale NiAl intermetallic compound precipitated during direct aging treatment. This process led to an exceptional combination of mechanical properties, achieving strength exceeding 2 GPa, elongation around 8%, and significantly reduced raw material cost compared with other maraging steels. To investigate the influence of Mo content on the precipitation behavior, microstructure, and mechanical properties of 13Ni maraging steel, Fonseca *et al.* [29] used a combination of selected area electron diffraction (SAED) and high resolution transmission electron microscope (HRTEM) to examine the morphology and crystallography of the precipitates. The results showed that the Mo content affected the kind of precipitates generated during aging, and stable $Fe_2(Mo,Ti)$ Laves phase was precipitated after the initial formation of Ni_3Mo precipitates. Despite these advances, the complex formation mechanisms of intermetallic compounds and their influence on the mechanical properties of such steels have not yet been systematically summarized [30].

This work presents a comprehensive overview of recent advancements in UHS martensitic steel and the prevalent types of precipitates in UHSSs. The precipitates in UHSSs are categorized as carbides (MC, M_2C, and M_3C) or intermetallic compounds (NiAl, Ni_3X, Fe_2Mo), and an in-depth analysis is conducted on their effects on the strength of UHS martensitic steel, particularly on aspects such as processing, microstructure, and mechanical properties. In addition, the precipitation-strengthening mechanisms in UHS martensitic steel are discussed. Finally, a prospect for the future development of UHS martensitic steel is outlined to contribute to its development.

2. Precipitates of UHS martensitic steel

The excellent service properties of UHS martensitic steel are characterized primarily by its UHS. To improve its mechanical properties, researchers extensively studied the influencing factors of UHS. Optimal combinations of different alloying elements were utilized to achieve the desired mechanical properties and microstructure attributes, primarily through the formation of a martensitic matrix and enhancement via dispersed precipitates. Precipitation strengthening is the predominant method to enhance UHS, as illustrated in Fig. 1, where the common precipitates in UHS steels mainly consist of carbides and intermetallic compounds. This review underscores the recent advancements in the application of carbides and intermetallic compounds for precipitation strengthening in UHS martensitic steel.

2.1. MC precipitates

Characterized by the addition of minor quantities of alloying elements such as chromium (Cr), molybdenum (Mo), nickel (Ni), and vanadium (V), high-strength low-alloy

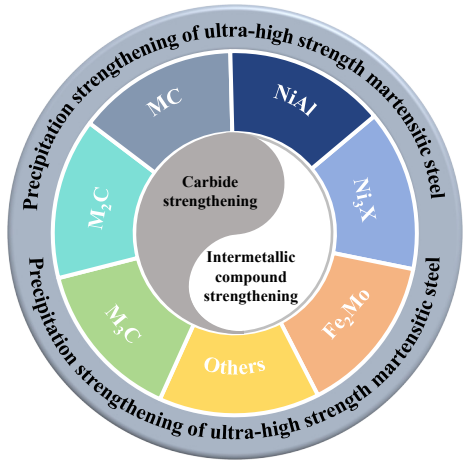

Fig. 1. Typical precipitates in UHS martensitic steel, including carbides (MC, M_2C, and M_3C) and intermetallic compounds (NiAl, Ni_3X, and Fe_2Mo).

(HSLA) steels are extensively utilized in marine engineering, naval ship structures, automotive sector, and infrastructure development. These steels are favored for their excellent combination of high strength, adequate toughness, favorable weldability, and good formability [31–37]. Microalloying, which involves the addition of niobium (Nb), V, and titanium (Ti), is a direct and economical production strategy for most HSLA steels. This method enables these steels to achieve outstanding mechanical properties through precipitation strengthening and grain refinement [38–40]. The precipitation mechanism of V, Ti, and Nb microalloyed steels is notably influenced by the addition of the alloying element Mo [32,41]. The introduction of Mo atoms in precipitated carbides contributes to precipitation strengthening by reducing the particle size and increasing the number density, thereby improving the overall material performance [42].

To investigate the precipitation evolution of MC carbides (M = Cr, Mo, V) in HSLA steels, Lu *et al.* [43] analyzed the microstructure of Cr–Ni–Mo–V alloyed HSLA steels using HRTEM. A diagram of the solution quenching and tempering (SQT) is illustrated in Fig. 2(a). According to the TEM observation, a significant number of MC nanoprecipitates, specifically V-rich particles, were randomly precipitated throughout the martensite matrix in the SQT samples, as depicted in Fig. 2(b1) and (b2). These precipitates were subsequently determined by HRTEM as MCs (M = Cr, Mo, V) with a face-centered cubic structure (Fig. 2(b3) and (b4)). According to the engineering stress–strain curves (Fig. 2(c1)), all the solution quenching and SQT samples showed continuous yielding. Compared with the solution quenching samples, the SQT samples exhibited a decrease in UTS but a significant increase in yield strength (YS) and total elongation (TE). With prolonged isothermal holding time (IHT), the YS and UTS of the SQT samples demonstrated a trend of initial increase and a subsequent decrease (Fig. 2(c2)). Optimal mechanical properties, including maximized YS and UTS, and sustained high TE were achieved at an IHT of 2 h. This finding was attributed to the small size and great quantity of MC precipitates in the SQT.

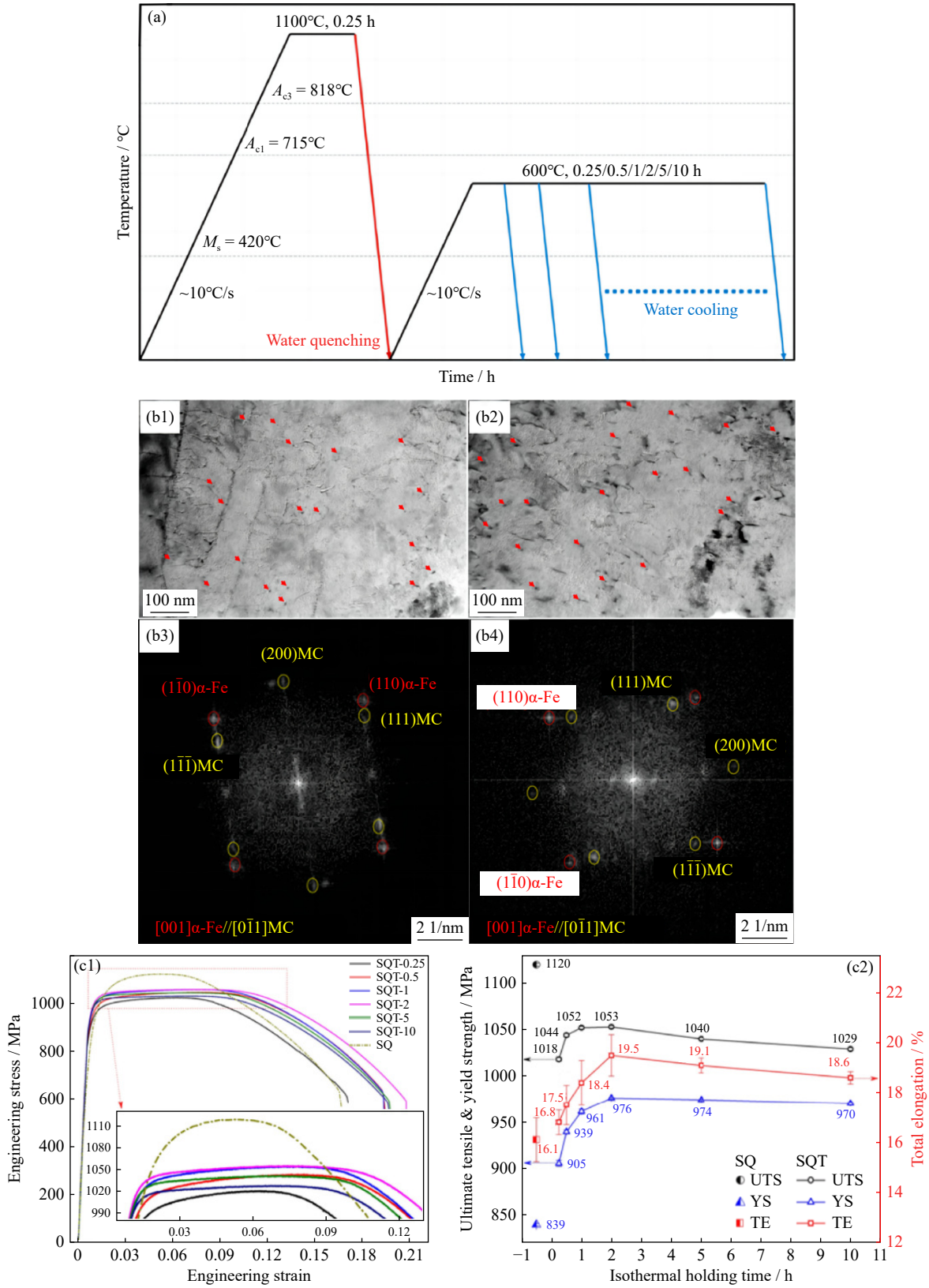

Fig. 2. Microstructure, precipitates, and mechanical properties of Cr–Ni–Mo–V alloyed HSLA steels. (a) Schematic of solution quenching and tempering (A_{c1}, A_{c3}, and M_s are the critical phase transformation temperatures); TEM images (b1, b2) of precipitates in SQT samples with IHT of (b1) 0.25 and (b2) 2 h and fast Fourier transformation (FFT) diagrams (b3, b4) of precipitates in the SQT samples with IHT of (b3) 0.25 and (b4) 2 h; engineering stress–strain curves of the SQT samples (c1) and variations in mechanical properties with IHT under SQT heat treatment (c2) [43]. Reprinted from *Mater. Sci. Eng. A*, Vol. 881, J. Lu, S.Z. Wang, H. Yu, *et al.*, Effect of precipitation on the mechanical behavior of vanadium micro-alloyed HSLA steel investigated by microstructural evolution and strength modeling, 145313, Copyright 2023, with permission from Elsevier.

2.2. M_2C precipitates

The mechanical properties of steel are predominantly affected by the alloying elements and the heat treatment. For a given alloy system, thermal treatments are a highly available approach for improving the performance of steels [44–45]. Cryogenic treatment is vital in refining the substructures of the matrix, modifying the carbide precipitates, and eliminating crystal defects [46–56].

To study the influence of secondary cryogenic treatment on the precipitation and mechanical properties, Yang *et al.* [57] subjected Ferrium S53 steel to single and double cryogenic treatments and analyzed its microstructure and mechanical properties. The route of the secondary cryogenic treatment is illustrated in Fig. 3(a), where the secondary aging treatment (SAT) samples subjected to the cryogenic treatment and two-pass cryogenically treated were denoted as SC-SAT and DC-SAT samples, respectively. The TEM and HRTEM images of the DC-SAT sample are depicted in Fig. 3(b1)–(b3). As shown in the dark-field TEM (DF-TEM) image of the DC-SAT sample (Fig. 3(b1)), substantial secondary precipitates were uniformly dispersed at the martensitic

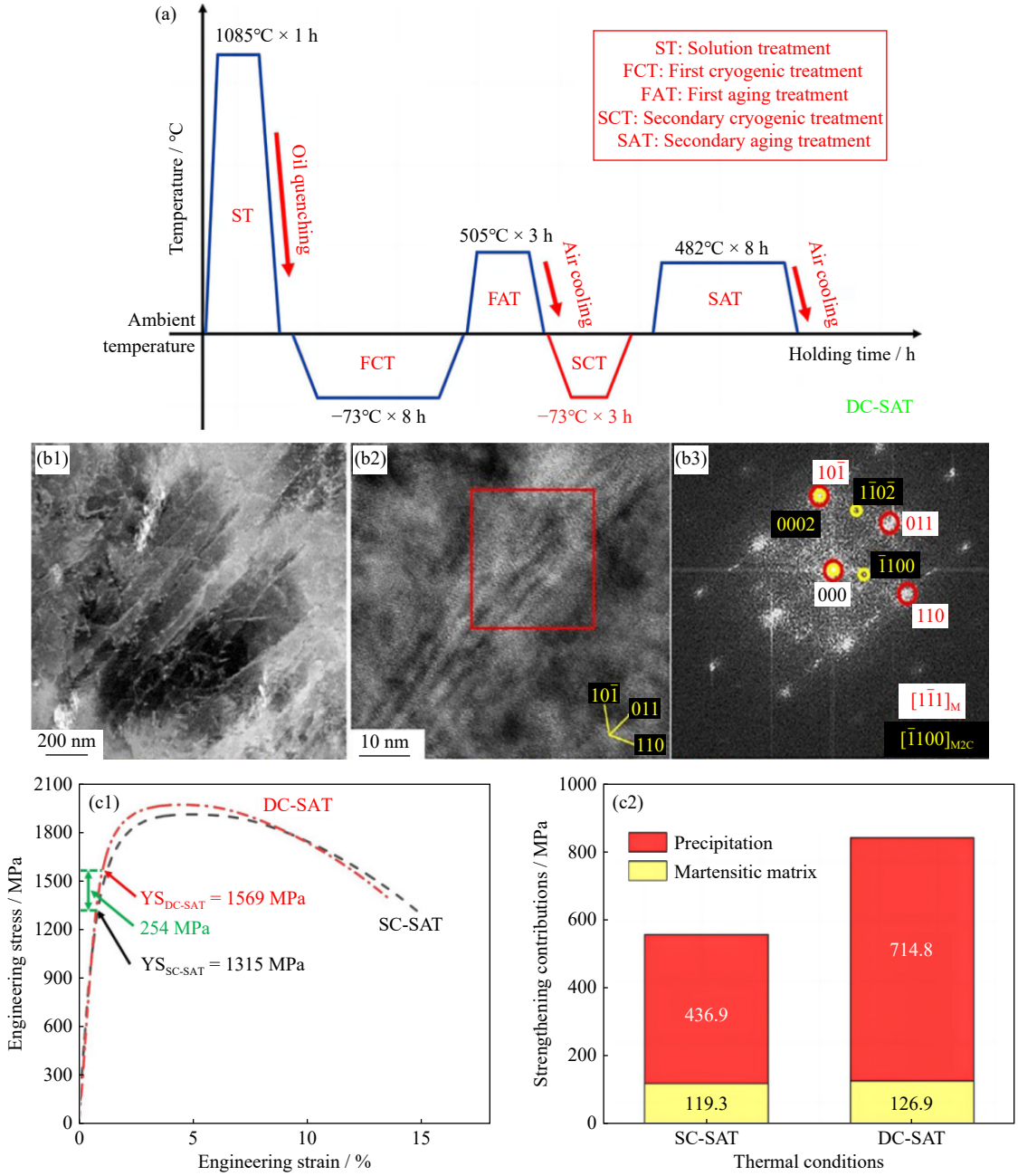

Fig. 3. Microstructure, precipitates, and mechanical properties in Ferrium S53 UHS stainless steel. (a) Schematic of the secondary cryogenic treatment; TEM and HRTEM images of DC-SAT sample: (b1) DF image, (b2) HRTEM image, and (b3) corresponding indexing result of FFT patterns obtained from the red rectangular region in (b2); engineering stress–strain curves of the two samples (c1) and contributions of precipitation strengthening and martensitic matrix strengthening (c2) [57]. Reprinted from *Mater. Charact.*, Vol. 178, Z. Yang, Z.B. Liu, J.X. Liang, Z.Y. Yang, and G.M. Sheng, Elucidating the role of secondary cryogenic treatment on mechanical properties of a martensitic ultra-high strength stainless steel, 111277, Copyright 2021, with permission from Elsevier.

lath boundaries and interiors. The indexed results of the FFT pattern obtained from the red rectangular region in Fig. 3(b2) are shown in Fig. 3(b3), the precipitates in the secondary aged steels were M_2C carbides. Fig. 3(c1) illustrates the engineering strain–stress curves of both samples. The yield strength of the DC-SAT sample showed a notable increase of 254 MPa compared with that of the SC-SAT sample, and the UTS approached nearly 2 GPa. However, the toughness remained similar between the two samples. Microstructural analysis revealed significant changes in the two key factors contributing to steel strength, namely, martensitic matrix and M_2C carbides. Therefore, the observed variation in yield strength was mainly attributed to the differences in precipitation strengthening and martensitic matrix strengthening between the two samples. As illustrated in Fig. 3(c2), the calculated contributions of precipitation strengthening to the yield strength of the two samples were 436.9 and 714.8 MPa, respectively. The enhanced precipitation-strengthening effect on the DC-SAT sample was mainly attributed to the formation of fine M_2C particles facilitated by the secondary cryogenic treatment.

2.3. M_3C precipitates

The pursuit of UHSSs with excellent toughness is a primary objective for metal structural materials. However, strength and toughness are usually mutually exclusive in steels; that is, an increase in strength typically results in a reduction in toughness. Extensive research efforts have been dedicated to developing UHSSs with sufficient toughness [58–63].

In recent years, HSLA steels have received growing interest due to their cost-effectiveness. To balance costs while achieving high strength and toughness, Wang *et al.* [64] employed tempforming and reheating (TFR) to produce UHS high-carbon martensitic steel and investigated the influence of its microstructure on its mechanical properties. The processing routes of TFR are shown in Fig. 4(a), with the samples designated as TFR3, TFR5, and TFR15. The precipitation of nanocarbides in the martensitic matrix was analyzed by HRTEM, as illustrated in Fig. 4(b1)–(b2). The corresponding electron diffraction pattern obtained from Fig. 4(b1) through FFT conversion is shown in Fig. 4(b2). FFT pattern analysis identified the precipitates as the Fe_3C phase. The engineering stress–strain curves of the samples are presented in Fig. 4(c1). The TFR3 sample demonstrated exceptional mechanical properties with a UTS of 2613 MPa, a YS of 2367 MPa, and a TE of 7%. Increasing the reheating time to 5 min resulted in a 5% decrease in total elongation. Meanwhile, the UTS (2593 MPa) and YS (2316 MPa) remained nearly unchanged compared with those of TFR3. Extending the reheating time to 15 min caused the TFR15 sample to fracture before reaching the yield point and exhibit no plastic deformation and a fracture stress of 1326 MPa. Compared with those at the rolling state, the yield strength and UTS of TFR3 steel increased by 713 and 918 MPa, respectively. The high strength of the TFR3 sample was mainly due to the nanoscale Fe_3C precipitated during tempering. Furthermore, a comparison of mechanical properties between the TFR steels and other UHSSs indicated that the TFR steels possessed the highest UTS while maintaining sufficient total elongation (Fig. 4(c2)).

2.4. NiAl precipitates

Uniform nanoparticle precipitation is a highly effective approach for enhancing the strength of low-carbon steels, with a strong reliance on the microstructure and the characteristics of precipitates such as morphology, size, number density, and structure [65–66]. For an optimal combination of high strength, excellent toughness, and good weldability, martensite is deemed the most suitable matrix, and the NiAl intermetallic compound is an effective strengthening phase [67–73].

To investigate NiAl precipitates and their influence on the mechanical properties of steel, Yang *et al.* [74] conducted an aging treatment on quenched 2.5Mn–1.5Cu–5.0Ni–1.0Al steel at different temperatures and analyzed its microstructure and mechanical properties. A diagram of the heat treatment process is illustrated in Fig. 5(a), and the samples with different aging temperatures were designated as QT500, QT550, QT600, and QT650. The microstructure of the nanoprecipitates in the QT500 sample was validated using HRTEM, revealing its numerous small ellipsoidal and spherical nanoprecipitates (Fig. 5(b1)–(b3)). Fig. 5(b1) illustrates the microstructure of a typical ellipsoidal nanoprecipitate. The B2-ordered structure of the ellipsoidal nanoprecipitates was confirmed by FFT and the corresponding inverse FFT, as illustrated in Fig. 5(b2) and (b3), respectively. The superlattice diffraction spots further indicated the precipitation of the NiAl intermetallic compound. Fig. 5(c1)–(c2) illustrates the mechanical properties of the steels under different heat treatments. As shown in Fig. 5(c1), aging at 500°C resulted in a significant increase in Vickers hardness to HV 497, which then decreased to a minimum of HV 327 at 650°C. The engineering stress–strain curves of the steels under different heat treatments are illustrated in Fig. 5(c2). After quenching, the steel showed a significant increase in yield strength and UTS. In particular, the UTS of QT500 steel was nearly 1.6 GPa, with a total elongation exceeding 11%. Meanwhile, the maximum yield strength of QT550 steel was almost 1.5 GPa, with a total elongation of nearly 10%. The precipitation-strengthening effect was evident in QT500 and QT550 steels, increasing their yield strengths to 481 and 508.5 MPa, respectively.

2.5. Ni_3X precipitates

The optimization of aging treatment is a highly effective method for manipulating the mechanical properties of maraging steels [75–77]. Increasing the aging temperature enhances toughness and ductility through the formation of lamellar or granular reversed austenite [78–79]. However, this method may be influenced by the coarsening of precipitates, leading to a substantial reduction in strength. This in-

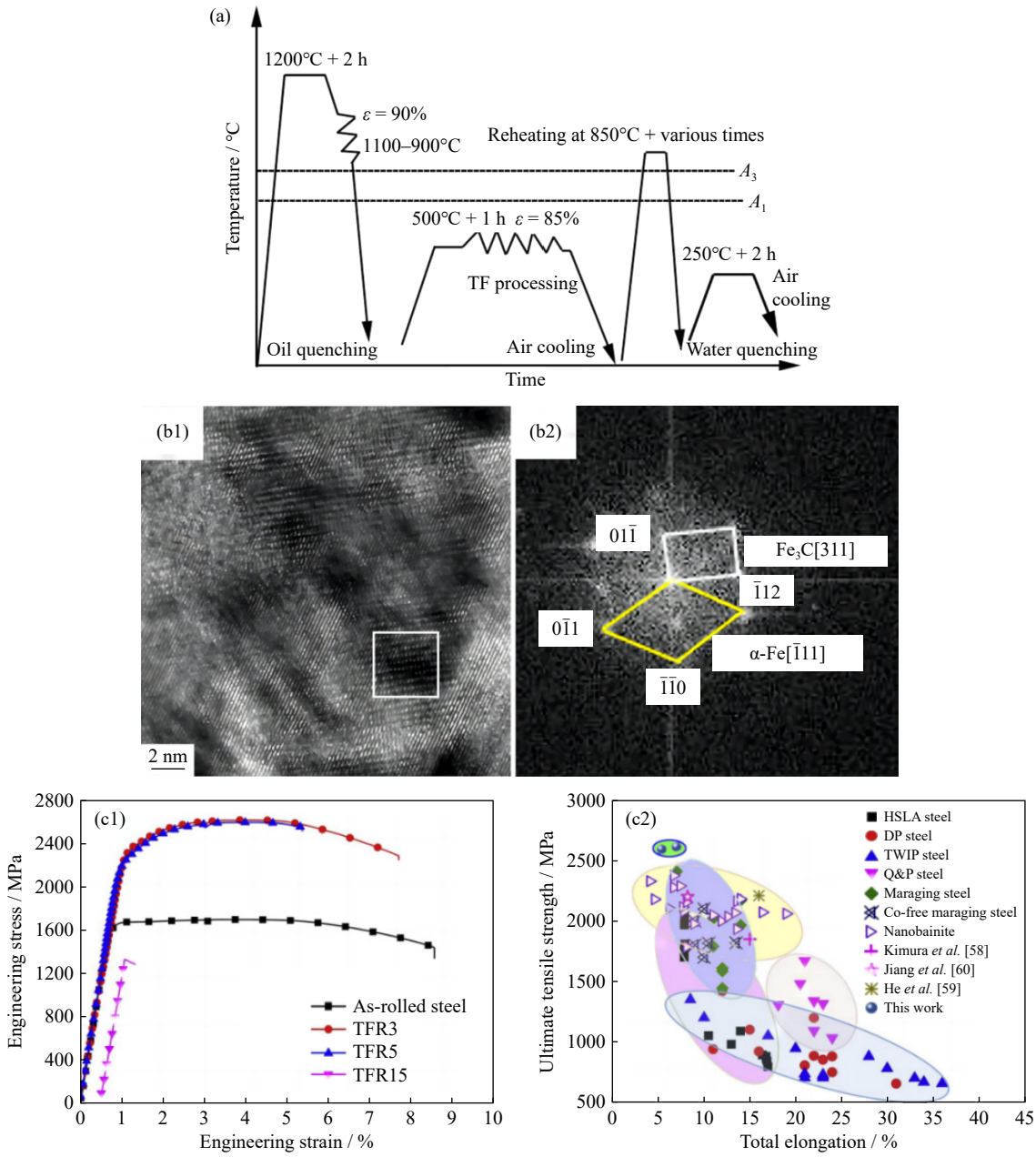

Fig. 4. Microstructure, precipitates, and mechanical properties in UHS high-carbon martensitic steel. (a) TFR route for producing UHS high-carbon martensitic steel (TF and ε represent tempforming and strain); HRTEM image and diffraction pattern of carbide precipitation in TFR steel: (b1) HRTEM image of martensite matrix and (b2) FFT diffraction pattern of (b1); engineering stress–strain curves of the samples (c1) and comparative analysis of mechanical properties between TFR steels and other UHSSs (c2) [64]. Reprinted from *Acta Mater.*, Vol. 158, Y.J. Wang, J.J. Sun, T. Jiang, Y. Sun, S.W. Guo, and Y.N. Liu, A low-alloy high-carbon martensite steel with 2.6 GPa tensile strength and good ductility, 247-256, Copyright 2018, with permission from Elsevier.

verse correlation stems from the different dynamics of precipitates and reversed austenite formation during aging [80].

To investigate the effect of aging temperature on the precipitates and mechanical properties of maraging steels, Zhang *et al.* [81] thoroughly analyzed the microstructure of 12Cr–10Ni–Mo–Ti cryogenic maraging steel using TEM and HRTEM. The dilatometric curve and diagram of the heat treatment route are illustrated in Fig. 6(a1) and (a2), with the steels subjected to varying aging temperatures denoted as A440, A500, A560, and A600. As shown by the DF-TEM image in Fig. 6(b1), a substantial number of rod-like particles were precipitated within the martensite laths. Lath-like reversed austenite structures were also formed at the boundaries of the laths. The rod-like precipitates were subsequently determined to be η-Ni_3(Ti,Al) precipitates on the basis of the HRTEM image in Fig. 6(b2). Fig. 6(c1)–(c2) illustrates the true stress–strain curves and strain-hardening rate curves of the samples. At room temperature, the solution-annealed (SA) sample exhibited a relatively soft behavior characterized by a yield strength of approximately 600 MPa and a total elongation of around 8% (Fig. 6(c1)). Following aging treatment, the yield strength significantly increased and reached approximately 1000 MPa for the A440 and A500 samples. Conversely, the A560 sample had softened and displayed a

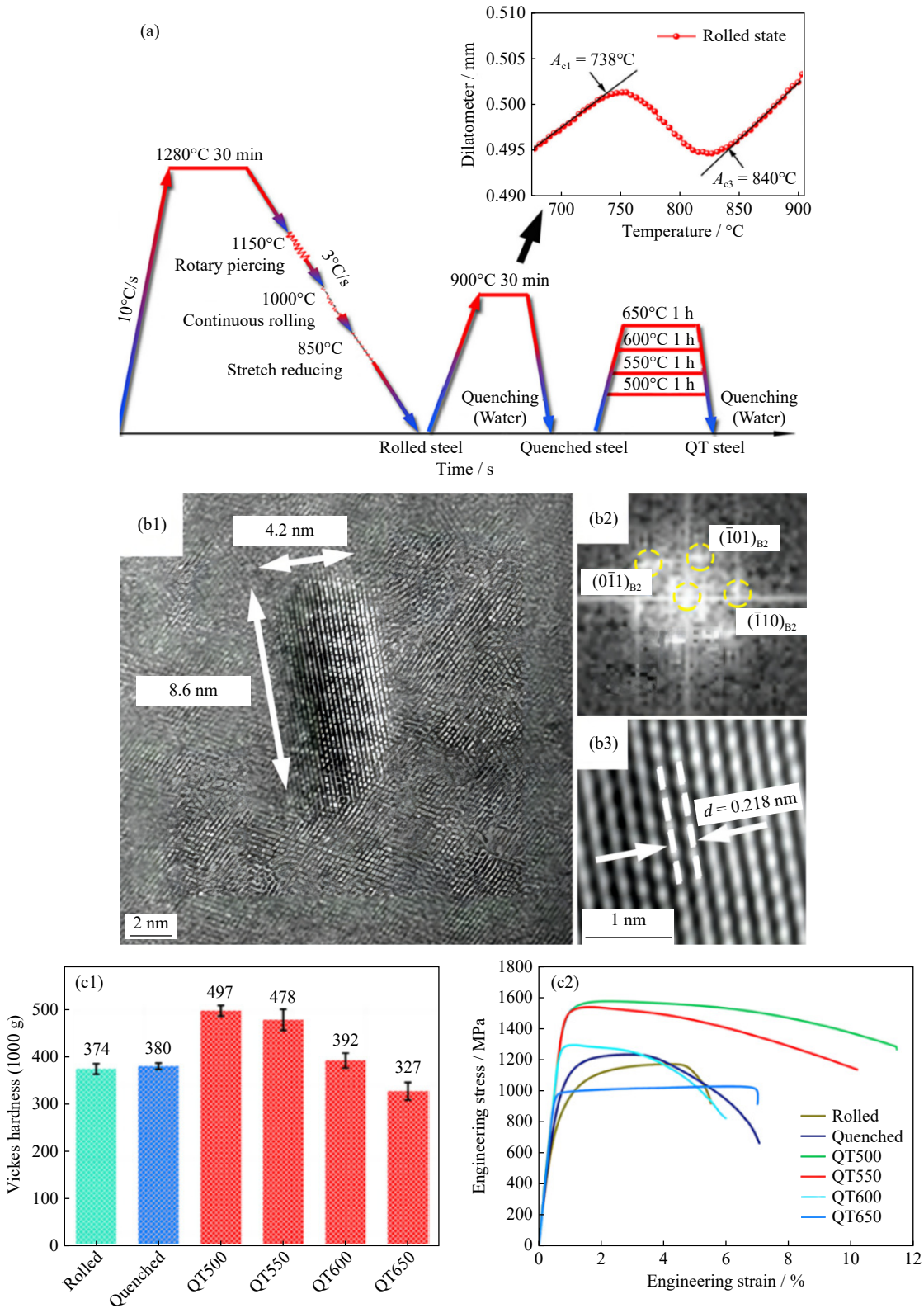

Fig. 5. Microstructure, precipitates, and mechanical properties in low-carbon UHS seamless tube steel. (a) Schematic of the heat treatment for steels; HRTEM images of precipitates when aged at 500°C: (b1) microstructure of precipitates in QT500 steel and the corresponding FFT (b2) and inverse FFT (b3) patterns; mechanical properties of the steels: (c1) Vickers hardness and (c2) engineering stress–strain curve [74]. Reprinted from *Mater. Sci. Eng. A*, Vol. 872, X.C. Yang, X.J. Di, Q.Y. Duan, W. Fu, L.Z. Ba, and C.N. Li, Effect of precipitation evolution of NiAl and Cu nanoparticles on strengthening mechanism of low carbon ultra-high strength seamless tube steel, 144939, Copyright 2023, with permission from Elsevier.

reduced yield strength of approximately 850 MPa but a comparatively high total elongation of 20%. Further aging at 600°C notably reduced the yield strength to 550 MPa. The relative change of yield strength at cryogenic temperature exhibited a similar trend, with a peak value of approximately 1400 MPa and a great total elongation of 26% observed in

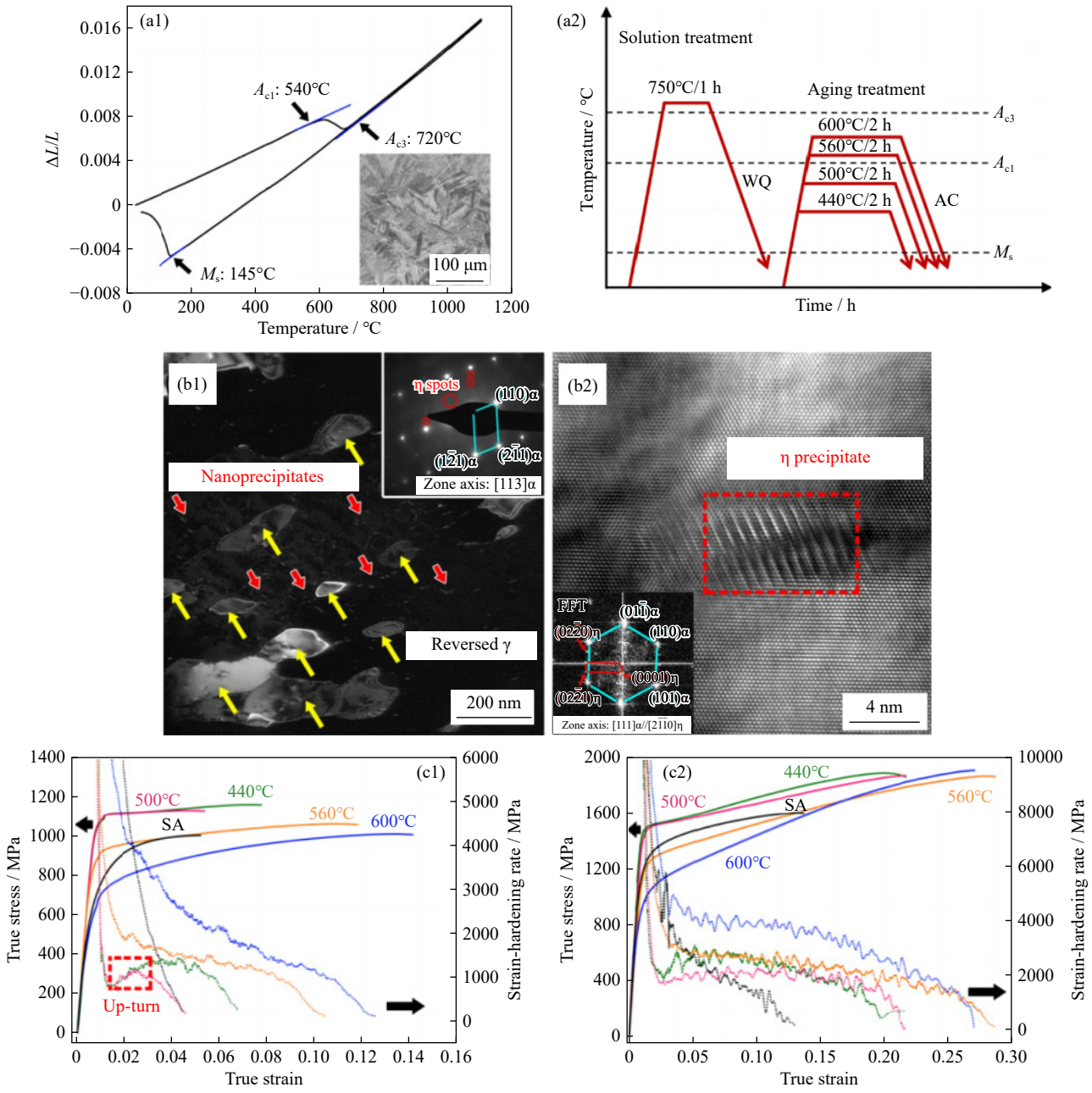

Fig. 6. Microstructure, precipitates, and mechanical properties of 12Cr–10Ni–Mo–Ti maraging steel. Dilatometric curve of the steel (a1) and schematic of the heat treatment process (a2) (WQ and AC represent water quenching and air cooling); DF-TEM images of the A500 sample (b1) and HRTEM image of η-Ni_3(Ti,Al) precipitates (b2) in the A500 sample; true stress–strain and strain-hardening rate curves of the samples tested at (c1) 25 and (c2) −196°C [81]. Reprinted by permission from Springer Nature: *J. Mater. Sci.*, Effect of aging temperature on the heterogeneous microstructure and mechanical properties of a 12Cr–10Ni–Mo–Ti maraging steel for cryogenic applications, H.L. Zhang, M.Y. Sun, D.P. Ma, *et al.*, Copyright 2021.

the A440 and A500 samples (Fig. 6(c2)). The aging temperature of 500°C was conducive to obtaining the desired microstructure, which is mainly composed of reversed austenite and η-Ni_3(Ti,Al) precipitates and exhibits good comprehensive mechanical properties. In addition, the precipitation-strengthening effect caused by η-Ni_3(Ti,Al) precipitates was quantified as 443 MPa.

2.6. Fe_2Mo precipitates

One main factor contributing to improved material properties is the precipitation strengthening caused by Mo-rich precipitates. For maraging steels, their strength is commonly enhanced through the precipitation of intermetallic compounds such as Ni_3Mo, Fe_2Mo, and Fe_7Mo_6 [82–88].

To investigate the mechanical properties, phase composition, and microstructure of high-Mo maraging steel coating, Xu *et al.* [89] selected a maraging steel powder with a high molybdenum content and employed laser cladding to prepare the coating at four different scanning speeds, designating the samples as S1, S2, S3, and S4. The schematic of the laser cladding process is illustrated in Fig. 7(a1). Fig. 7(a2) shows the XRD patterns of the samples, which mainly consisted of α-Fe and γ-Fe phases. In addition, the diffraction peaks of the Fe_2Mo phase were observed, especially promin-

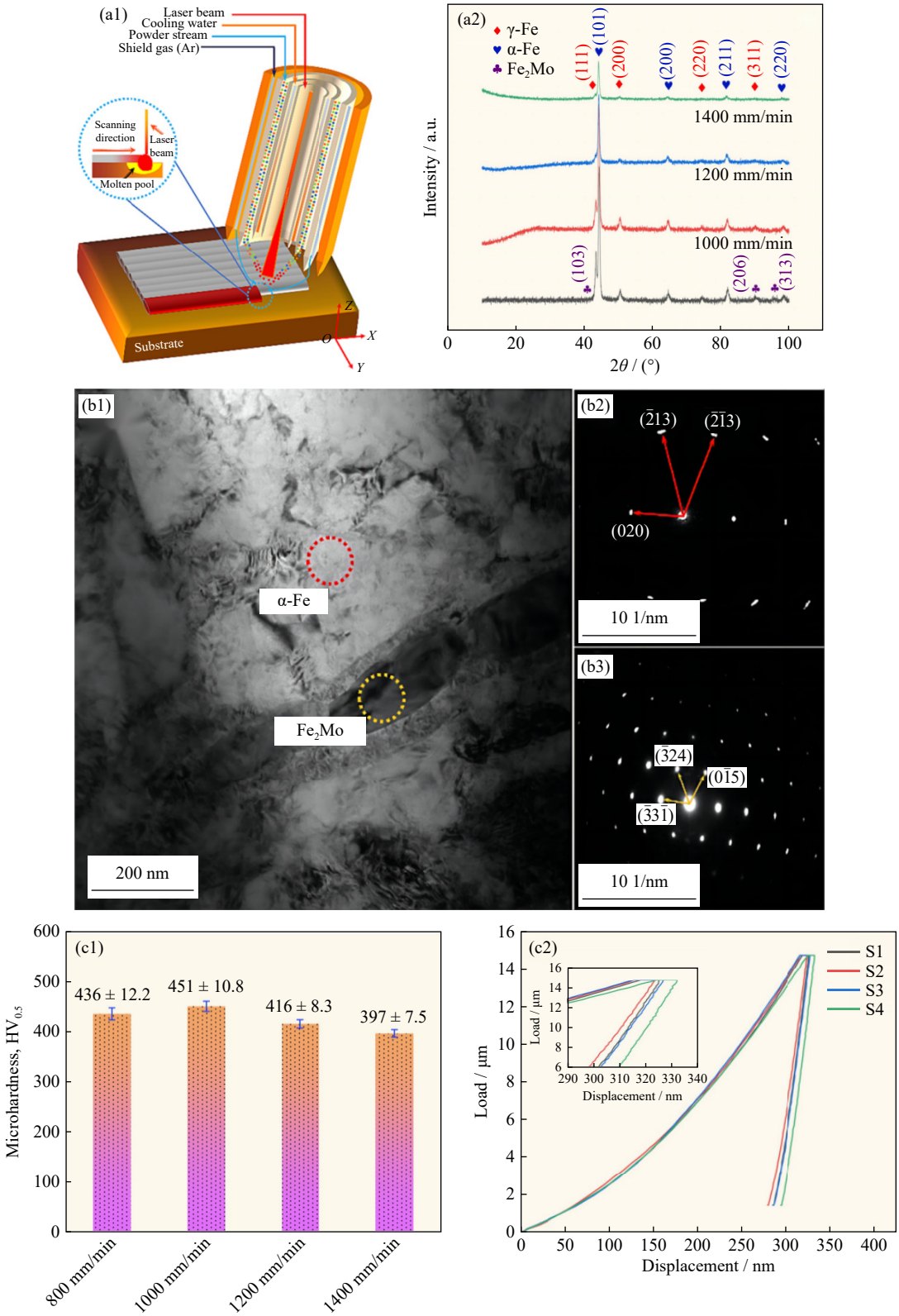

Fig. 7. Microstructure, precipitates, and mechanical properties of maraging steel coatings. Schematic of laser cladding process (a1) and XRD patterns of the samples (a2); TEM image of the S2 sample (b1) and corresponding SAED patterns of martensite (b2) and Fe_2Mo (b3); surface microhardness of the samples (c1) and load–displacement curves of the samples (c2) [89]. Reprinted from *Mater. Charact.*, Vol. 205, T.Z. Xu, S. Zhang, L. Wang, *et al.*, Influence of scanning speed on the microstructure, nanoindentation characteristics and tribological behavior of novel maraging steel coatings by laser cladding, 113335, Copyright 2023, with permission from Elsevier.

ently in the S1 and S2 samples. However, as the scanning speed increased, the Fe_2Mo peaks gradually weakened and eventually disappeared in the S3 and S4 samples. Fig. 7(b1) illustrates the TEM image of the S2 coating, showing distinct

black-striped precipitates alongside the white matrix phase. Additional details regarding the phase structure were obtained through SAED analysis, as depicted in Fig. 7(b2) and (b3). The bright white matrix phase was identified as martensite, which has a body-centered cubic structure. By contrast, the dense hexagonal structure observed in the black-striped precipitates suggests the existence of the Fe_2Mo phase. Fig. 7(c1) illustrates the microhardness of the samples measured at $HV_{0.5}$ (436 ± 12.2), (451 ± 10.8), (416 ± 8.3), and (397 ± 7.5). Among the samples, S2 exhibited the highest microhardness. Fig. 7(c2) presents the load–displacement curves of the samples. Their maximum indentation depths (d_{max}) were 325.25, 322.88, 326.52, and 337.78 nm. The reduction in d_{max} indicated an enhancement of the coating hardness. The high hardness of the S2 sample was primarily attributed to the precipitation-strengthening effect. During the solidification, the Mo atoms in the sample precipitated between the dendrites, leading to the formation of the Fe_2Mo phase. This intermetallic compound significantly enhanced the precipitation-strengthening effect on the coating and thereby substantially improved the mechanical properties.

2.7. Other precipitates

In addition to the above common precipitates, UHS martensitic steel contains other carbides and intermetallic compounds. For example, El-Meligy *et al.* [90] studied the influence of different tungsten contents on the microstructure and mechanical properties of UHSS and found that needle-like nanocarbides with a diameter of 50 nm were densely packed and situated between the fine martensite laths. With a tungsten addition of up to 1.6wt%, the strength increased. However, when tungsten content was raised to 2wt%, the strength and ductility decreased. Therefore, tungsten at a level of 1.6wt% may dissolve and incorporate into the carbide lattice, forming $Cr_{21}W_2C_6$. However, tungsten at high contents cannot be dissolved into the carbide lattice and might instead be accommodated in the iron lattice in its elemental form, leading to reduced strength and deteriorated ductility. The synergistic combination of small martensite laths, nanosized residual austenite films, and densely packed needle-like nanocarbides collaboratively contributed to the UHS. Yang *et al.* [91] extensively investigated a 12Mn maraging steel using various experimental techniques, including electron backscattered diffraction (EBSD), TEM, and mechanical property testing. Their study revealed that the primary strengthening phase in the aged alloy at 450°C was the Fe_2TiSi phase precipitating in the martensite. Reversed austenite was also observed between the martensite laths, significantly contributing to the steel's toughness. Through the meticulous optimization of the aging process parameters, the 12Mn maraging steel achieved a high UTS of approximately 1700 MPa and a total elongation of approximately 7%. Cu precipitates also play a significant role in the strengthening of UHS martensitic steel. Zhang *et al.* [92] investigated the microstructure and nanoscale Cu precipitates in Cu-bearing HSLA steel using SEM, EBSD, HRTEM, and APT. Their findings demonstrated that the aging conditions facilitating average precipitation of 1wt% Cu can enhance the strength by approximately 172 MPa.

3. Discussion

After years of development, UHS martensitic steel has achieved high strength with good elongation. In previous sections, the precipitates in UHS martensitic steel and their precipitation-strengthening effects are examined. The significant strengthening effect in UHS martensitic steel mainly originates from the interaction between the precipitates and dislocations. As illustrated in Fig. 8, the two primary mechanisms of interaction between dislocations and precipitates are dislocation–bypass and dislocation–cutting [93]. When the precipitate size is small and remains coherent with the matrix, dislocations cut through the precipitates. As the precipitate phase grows and loses coherence with the matrix, dislocations tend to bypass the precipitates. The precipitates in UHS martensitic steel are predominantly alloy carbides and single-phase semicoherent or incoherent intermetallic compounds. Therefore, most of them adhere to the bypass

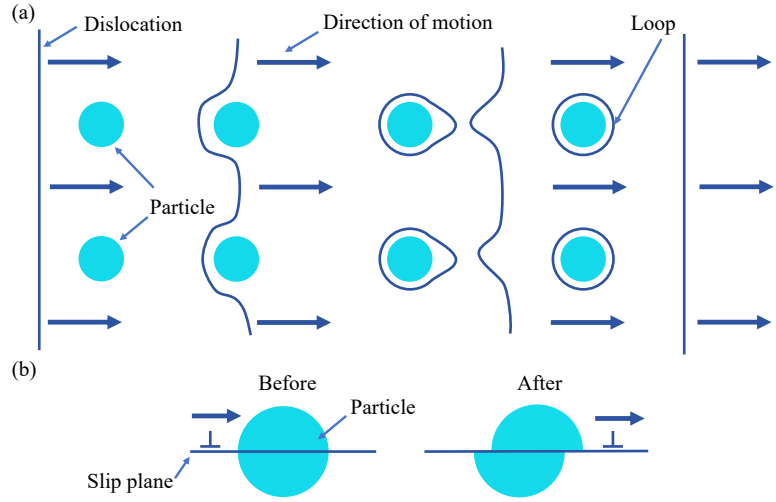

Fig. 8. Schematic of the interaction mechanism between the precipitates and dislocations: (a) dislocation–bypass mechanism; (b) dislocation–cutting mechanism.

mechanism. Some intermetallic compounds with small sizes maintain good coherence with the matrix, such as NiAl, and thus adhere to the cutting mechanism. Nevertheless, the critical transition size of the precipitate phase for these two mechanisms remains controversial [94–95] and requires further in-depth studies in the future.

Enhancing the toughness of UHS martensitic steel while maintaining its high strength is paramount. For example, the toughness can be improved by adjusting the size, morphology, and distribution of carbides. Han *et al.* [96] found that uniformly distributed, short-rod-shaped $M_{23}C_6$ carbides (with sizes less than 100 nm), and spherical MC carbides (with diameters ranging from a few nanometers to approximately 20 nm) contribute to a balance between high strength and high toughness. Conversely, toughness is compromised by the presence of high-density, large M_3C carbides (with lengths and widths of approximately 200–500 nm and 20–50 nm, respectively). Xie *et al.* [97] also observed that toughness is enhanced by fine, uniformly distributed nanocarbides but adversely affected by large, coarse carbides.

This review also compiles data on the recent occurrence frequency of precipitates for precipitation strengthening in UHS martensitic steel. As shown in Fig. 9, the common precipitates in UHS martensitic steel include carbides and intermetallic compounds. In particular, the frequency of intermetallic compound strengthening is the highest, indicating that the development of intermetallic compounds with enhanced precipitation-strengthening effects holds great potential. In the development of UHS martensitic steel with outstanding comprehensive properties, the focus should not only be on the size and type of precipitates. Regulating the size, content, and stability of metastable austenite and optimizing the structures of martensite and austenite and the substructure of dislocations are necessary to achieve a balance between UHS and excellent plasticity and toughness.

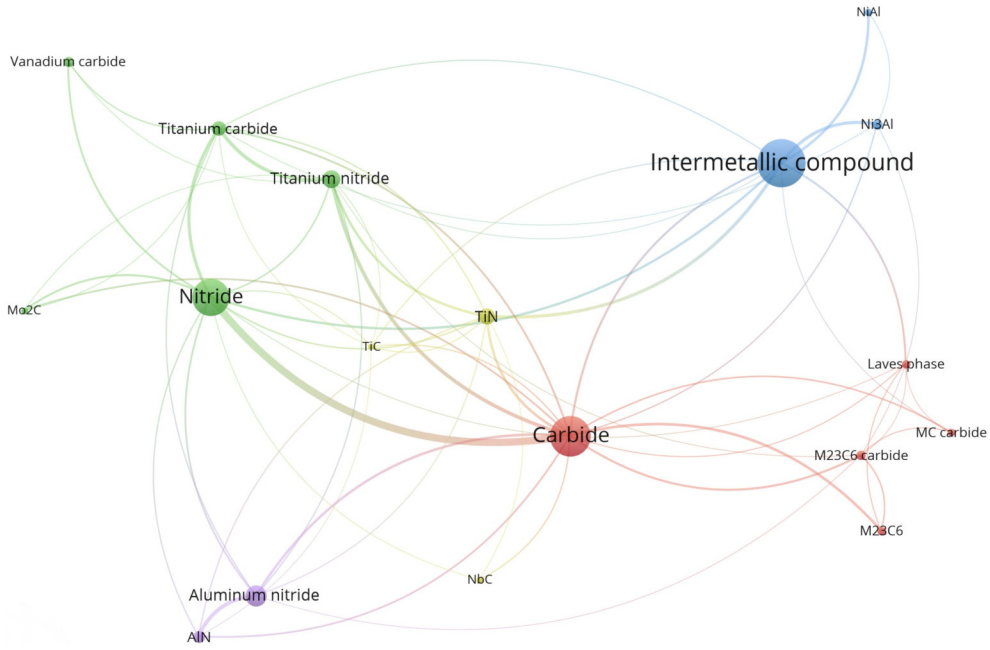

Fig. 9. Network visualization of keywords "UHS martensitic steel, precipitation strengthening" in literature from the Web of Science database.

4. Conclusions and perspectives

Owing to its exceptional strength, UHS martensitic steel is extensively utilized in critical components across various industries, including aviation, shipbuilding, and engineering machinery. Precipitation strengthening plays a crucial role in the enhancement of this strength, predominantly through the interactions of dislocations with precipitated carbides and/or intermetallic compounds. The current trends in the ongoing development of UHS martensitic steel are as follows.

(1) Coprecipitation of carbides and intermetallic compounds: The strength of UHS martensitic steel can be strengthened by the coprecipitation of nanoscale carbides and intermetallic compounds. This strategy effectively combines multiple precipitates, resulting in enhanced strengthening and toughening effects compared with single-type nanoprecipitates.

(2) Comprehensive databases for UHS martensitic steel: Given the significant variations among different types of UHS martensitic steel and the lack of high-quality data, a comprehensive database must be urgently developed. This resource would include chemical compositions, processing methods, precipitate types, and mechanical properties to support research and development efforts.

(3) High-throughput computational techniques for UHS martensitic steel: High-throughput materials integrated with computational technology are being leveraged to enhance precision and shorten development cycles in steel material research. This approach is particularly promising for advancing the study and application of UHS martensitic steel.

(4) Data-driven research and development strategies for UHS martensitic steel: The application of machine learning

to existing data on UHS martensitic steel allows for the design and development of new steel grades. These techniques establish quantitative relationships between key compositional and processing parameters and steel properties, aiding in the manufacture of UHS martensitic steel with optimized mechanical properties.

(5) Simultaneous improvement of the strength and toughness of UHS martensitic steel: Fine grain strengthening is employed to enhance the strength and toughness of UHS martensitic steel. Integrating traditional strengthening methods with nanotechnology also facilitates synergistic effects on strengthening and toughening. Precise control over the size, quantity, and distribution of nanocarbides and intermetallic compounds is crucial for this purpose.

By intensifying focus on these strategic areas, we can further advance the development of UHS martensitic steel to meet future industry demands.

Acknowledgements

This work was supported by the National Natural Science Foundation of China (Nos. 52122408 and 52071023). H.H. Wu also thanks the financial support from the Fundamental Research Funds for the Central Universities (University of Science and Technology Beijing, No. FRF-TP-2021-04C1, and 06500135). The computing work was supported by USTB MatCom of Beijing Advanced Innovation Center for Materials Genome Engineering.

Conflict of Interest

Xinping Mao and Honghui Wu are an advisory member and an editorial board member for this journal, respectively, and were not involved in the editorial review or the decision to publish this article. The authors declare that they have no known competing financial interests or personal relationships that could have appeared to influence the work reported in this paper.

References

[1] H. Dong, X.T. Lian, C.D. Hu, *et al*., High performance steels: The scenario of theory and technology, *Acta Metall. Sin.*, 56(2020), No. 4, p. 558.

[2] I. Nedelcu and I. Carceanu, Some aspects concerning the mechanism of hardening of maraging 300 steel, *Metall. Int.*, 18(2013), p. 95.

[3] A.K. da Silva, I.R.S. Filho, W. Lu, *et al*., A sustainable ultrahigh strength Fe18Mn3Ti maraging steel through controlled solute segregation and α-Mn nanoprecipitation, *Nat. Commun.*, 13(2022), No. 1, art. No. 2330.

[4] D.P.M. da Fonseca, A.L.M. Feitosa, L.G. de Carvalho, R.L. Plaut, and A.F. Padilha, A short review on ultra-high-strength maraging steels and future perspectives, *Mater. Res.*, 24(2021), No. 1, art. No. e20200470.

[5] T.J.B. Alves, G.C.S. Nunes, L.F.S. Tupan, *et al*., Aging-induced transformations of maraging-400 alloys, *Metall. Mater. Trans. A*, 49(2018), No. 8, p. 3441.

[6] U.K. Viswanathan, G.K. Dey, and M.K. Asundi, Precipitation hardening in 350 grade maraging steel, *Metall. Trans. A*, 24(1993), No. 11, p. 2429.

[7] Y. He, K. Yang, W.S. Qu, F.Y. Kong, and G.Y. Su, Strengthening and toughening of a 2800-MPa grade maraging steel, *Mater. Lett.*, 56(2002), No. 5, p. 763.

[8] Y. He, K. Yang, W. Sha, and D.J. Cleland, Microstructure and mechanical properties of a 2000 MPa Co-free maraging steel after aging at 753 K, *Metall. Mater. Trans. A*, 35(2004), No. 9, p. 2747.

[9] W. Xu, P.E.J. Rivera-Díaz-del-Castillo, W. Wang, *et al*., Genetic design and characterization of novel ultra-high-strength stainless steels strengthened by Ni_3Ti intermetallic nanoprecipitates, *Acta Mater.*, 58(2010), No. 10, p. 3582.

[10] Y.P. Zhang, D.P. Zhan, X.W. Qi, and Z.H. Jiang, Austenite and precipitation in secondary-hardening ultra-high-strength stainless steel, *Mater. Charact.*, 144(2018), p. 393.

[11] H.L. Zhang, G.Q. Zhang, H.C. Zhou, *et al*., Influence of cooling rate during cryogenic treatment on the hierarchical microstructure and mechanical properties of M54 secondary hardening steel, *Mater. Sci. Eng. A*, 851(2022), art. No. 143659.

[12] X.Y. Li, Z.H. Zhang, L.J. Liu, *et al*., Structure transformations and mechanical properties of the ultra-high-strength M54 steel produced by spark plasma sintering, *Powder Metall. Met. Ceram.*, 61(2022), No. 1, p. 40.

[13] R. Veerababu, R. Balamuralikrishnan, and S. Karthikeyan, Nanoscale clusters in secondary hardening ultra-high strength steels with 1 and 3 wt% Mo: An atom probe investigation, *J. Mater. Res.*, 35(2020), No. 14, p. 1763.

[14] R. Veerababu, R. Balamuralikrishnan, K. Muraleedharan, and M. Srinivas, Investigation of clusters in medium carbon secondary hardening ultra-high-strength steel after hardening and aging treatments, *Metall. Mater. Trans. A*, 46(2015), No. 6, p. 2455.

[15] Y.K. Kim, K.S. Kim, Y.B. Song, J.H. Park, and K.A. Lee, 2.47 GPa grade ultra-strong 15Co–12Ni secondary hardening steel with superior ductility and fracture toughness, *J. Mater. Sci. Technol.*, 66(2021), p. 36.

[16] X.Y. Li, Z.H. Zhang, X.W. Cheng, G.J. Huo, Q. Song, and Y. Xu, Direct achievement of ultra-high strength and good ductility for high Co–Ni secondary hardening steel by combining spark plasma sintering and deformation, *Mater. Lett.*, 290(2021), art. No. 129465.

[17] Y.P. Zhang, D.P. Zhan, X.W. Qi, and Z.H. Jiang, Effect of solid-solution temperature on the microstructure and properties of ultra-high-strength ferrium S53® steel, *Mater. Sci. Eng. A*, 730(2018), p. 41.

[18] Y.B. Xiong, D.X. Wen, Z.Z. Zheng, and J.J. Li, Effect of interlayer temperature on microstructure evolution and mechanical performance of wire arc additive manufactured 300M steel, *Mater. Sci. Eng. A*, 831(2022), art. No. 142351.

[19] A. Bag, D. Delbergue, P. Bocher, M. Lévesque, and M. Brochu, Statistical analysis of high cycle fatigue life and inclusion size distribution in shot peened 300M steel, *Int. J. Fatigue*, 118(2019), p. 126.

[20] M.A.S. Torres and H.J.C. Voorwald, An evaluation of shot peening, residual stress and stress relaxation on the fatigue life of AISI 4340 steel, *Int. J. Fatigue*, 24(2002), No. 8, p. 877.

[21] S. Floreen, The physical metallurgy of maraging steels, *Metall. Rev.*, 13(1968), No. 1, p. 115.

[22] K. Manigandan, T.S. Srivatsan, D. Tammana, B. Poorganji, and V.K. Vasudevan, Influence of microstructure on strain-controlled fatigue and fracture behavior of ultra high strength alloy steel AerMet 100, *Mater. Sci. Eng. A*, 601(2014), p. 29.

[23] X.L. Wang, Z.J. Xie, X.C. Li, and C.J. Shang, Recent progress in visualization and digitization of coherent transformation structures and application in high-strength steel, *Int. J. Miner. Metall. Mater.*, 31(2024), No. 6, p. 1298.

[24] Z.P. Lu, S.H. Jiang, J.Y. He, *et al*., Second phase strengthening

in advanced metal materials, *Acta Metall. Sin.*, 52(2016), No. 10, p. 1183.
[25] J. Dong, X.S. Zhou, Y.C. Liu, C. Li, C.X. Liu, and Q.Y. Guo, Carbide precipitation in Nb–V–Ti microalloyed ultra-high strength steel during tempering, *Mater. Sci. Eng. A*, 683(2017), p. 215.
[26] Y.F. Li, X. Cheng, D. Liu, and H.M. Wang, Influence of last stage heat treatment on microstructure and mechanical properties of laser additive manufactured AF1410 steel, *Mater. Sci. Eng. A*, 713(2018), p. 75.
[27] A. Mondiere, V. Déneux, N. Binot, and D. Delagnes, Controlling the MC and M_2C carbide precipitation in Ferrium® M54® steel to achieve optimum ultimate tensile strength/fracture toughness balance, *Mater. Charact.*, 140(2018), p. 103.
[28] X.D. Nong, X.J. Xiong, X. Gu, *et al*., A novel low-cost ultra-strong maraging steel by additive manufacturing, *Mater. Sci. Eng. A*, 887(2023), art. No. 145747.
[29] D.P.M. da Fonseca, M.V.P. Altoé, B.S. Archanjo, E. Annese, and A.F. Padilha, Influence of Mo content on the precipitation behavior of 13Ni maraging ultra-high strength steels, *Metals*, 13(2023), No. 12, art. No. 1929.
[30] M. Zhou, H.H. Wu, Y. Wu, *et al*., Phase field modeling of grain stability of nanocrystalline alloys by explicitly incorporating mismatch strain, *Rare Met.*, 43(2024), No. 7, p. 3370.
[31] D.C. Ramachandran, J. Moon, C.H. Lee, *et al*., Role of bainitic microstructures with M–A constituent on the toughness of an HSLA steel for seismic resistant structural applications, *Mater. Sci. Eng. A*, 801(2021), art. No. 140390.
[32] H.K. Dong, H. Chen, A.R. Khorasgani, *et al*., Revealing the influence of Mo addition on interphase precipitation in Ti-bearing low carbon steels, *Acta Mater.*, 223(2022), art. No. 117475.
[33] L.Y. Kan, Q.B. Ye, Z.D. Wang, and T. Zhao, Improvement of strength and toughness of 1 GPa Cu-bearing HSLA steel by direct quenching, *Mater. Sci. Eng. A*, 855(2022), art. No. 143875.
[34] C. Ledermueller, H.I. Pratiwi, R.F. Webster, M. Eizadjou, S.P. Ringer, and S. Primig, Microalloying effects of Mo versus Cr in HSLA steels with ultrafine-grained ferrite microstructures, *Mater. Des.*, 185(2020), art. No. 108278.
[35] Z.D. Wang, G.F. Sun, M.Z. Chen, *et al*., Investigation of the underwater laser directed energy deposition technique for the on-site repair of HSLA-100 steel with excellent performance, *Addit. Manuf.*, 39(2021), art. No. 101884.
[36] J. Lu, H. Yu, and S.F. Yang, Mechanical behavior of multi-stage heat-treated HSLA steel based on examinations of microstructural evolution, *Mater. Sci. Eng. A*, 803(2021), art. No. 140493.
[37] Z. Cheng, S.Z. Wang, G.L. Wu, J.H. Gao, X.S. Yang, and H.H. Wu, Tribological properties of high-entropy alloys: A review, *Int. J. Miner. Metall. Mater.*, 29(2022), No. 3, p. 389.
[38] S. Vervynckt, K. Verbeken, B. Lopez, and J.J. Jonas, Modern HSLA steels and role of non-recrystallisation temperature, *Int. Mater. Rev.*, 57(2012), No. 4, p. 187.
[39] T.N. Baker, Microalloyed steels, *Ironmaking Steelmaking*, 43(2016), No. 4, p. 264.
[40] S.Z. Wang, Z.J. Gao, G.L. Wu, and X.P. Mao, Titanium microalloying of steel: A review of its effects on processing, microstructure and mechanical properties, *Int. J. Miner. Metall. Mater.*, 29(2022), No. 4, p. 645.
[41] C. Ioannidou, Z. Arechabaleta, A. Navarro-López, *et al*., Interaction of precipitation with austenite-to-ferrite phase transformation in vanadium micro-alloyed steels, *Acta Mater.*, 181(2019), p. 10.
[42] P. Gong, X.G. Liu, A. Rijkenberg, and W.M. Rainforth, The effect of molybdenum on interphase precipitation and microstructures in microalloyed steels containing titanium and vanadium, *Acta Mater.*, 161(2018), p. 374.
[43] J. Lu, S.Z. Wang, H. Yu, *et al*., Effect of precipitation on the mechanical behavior of vanadium micro-alloyed HSLA steel investigated by microstructural evolution and strength modeling, *Mater. Sci. Eng. A*, 881(2023), art. No. 145313.
[44] Y. Snir, S. Haroush, A. Dannon, A. Landau, D. Eliezer, and Y. Gelbstein, Aging condition and trapped hydrogen effects on the mechanical behavior of a precipitation hardened martensitic stainless steel, *J. Alloys Compd.*, 805(2019), p. 509.
[45] G.F. Pan, F.Y. Wang, C.L. Shang, *et al*., Advances in machine learning- and artificial intelligence-assisted material design of steels, *Int. J. Miner. Metall. Mater.*, 30(2023), No. 6, p. 1003.
[46] T. Sonar, S. Lomte, and C. Gogte, Cryogenic treatment of metal–A review, *Mater. Today Proc.*, 5(2018), No. 11, p. 25219.
[47] D. Das, A.K. Dutta, and K.K. Ray, Influence of varied cryotreatment on the wear behavior of AISI D2 steel, *Wear*, 266(2009), No. 1-2, p. 297.
[48] Z.J. Yan, K. Liu, and J. Eckert, Effect of tempering and deep cryogenic treatment on microstructure and mechanical properties of Cr–Mo–V–Ni steel, *Mater. Sci. Eng. A*, 787(2020), art. No. 139520.
[49] X.G. Yan and D.Y. Li, Effects of the sub-zero treatment condition on microstructure, mechanical behavior and wear resistance of W9Mo3Cr4V high speed steel, *Wear*, 302(2013), No. 1-2, p. 854.
[50] D. Das, A.K. Dutta, and K.K. Ray, Inconsistent wear behaviour of cryotreated tool steels: Role of mode and mechanism, *Mater. Sci. Technol.*, 25(2009), No. 10, p. 1249.
[51] P. Mónica, P.M. Bravo, and D. Cárdenas, Deep cryogenic treatment of HPDC AZ91 magnesium alloys prior to aging and its influence on alloy microstructure and mechanical properties, *J. Mater. Process. Technol.*, 239(2017), p. 297.
[52] T. Sonar, S. Lomte, C. Gogte, and V. Balasubramanian, Minimization of distortion in heat treated AISI D2 tool steel: Mechanism and distortion analysis, *Procedia Manuf.*, 20(2018), p. 113.
[53] M.A. Jaswin and D.M. Lal, Effect of cryogenic treatment on the tensile behaviour of En 52 and 21-4N valve steels at room and elevated temperatures, *Mater. Des.*, 32(2011), No. 4, p. 2429.
[54] A.Y.L. Yong, K.H.W. Seah, and M. Rahman, Performance of cryogenically treated tungsten carbide tools in milling operations, *Int. J. Adv. Manuf. Technol.*, 32(2007), No. 7, p. 638.
[55] K. Vadivel and R. Rudramoorthy, Performance analysis of cryogenically treated coated carbide inserts, *Int. J. Adv. Manuf. Technol.*, 42(2009), No. 3, p. 222.
[56] Z.J. Weng, K.X. Gu, K.K. Wang, X.Z. Liu, and J.J. Wang, The reinforcement role of deep cryogenic treatment on the strength and toughness of alloy structural steel, *Mater. Sci. Eng. A*, 772(2020), art. No. 138698.
[57] Z. Yang, Z.B. Liu, J.X. Liang, Z.Y. Yang, and G.M. Sheng, Elucidating the role of secondary cryogenic treatment on mechanical properties of a martensitic ultra-high strength stainless steel, *Mater. Charact.*, 178(2021), art. No. 111277.
[58] Y. Kimura, T. Inoue, F.X. Yin, and K. Tsuzaki, Inverse temperature dependence of toughness in an ultrafine grain-structure steel, *Science*, 320(2008), No. 5879, p. 1057.
[59] B.B. He, B. Hu, H.W. Yen, *et al*., High dislocation density-induced large ductility in deformed and partitioned steels, *Science*, 357(2017), No. 6355, p. 1029.
[60] S.H. Jiang, H. Wang, Y. Wu, *et al*., Ultrastrong steel via minimal lattice misfit and high-density nanoprecipitation, *Nature*, 544(2017), p. 460.
[61] J.J. Sun, Y.N. Liu, Y.T. Zhu,et al., Super-strong dislocation-structured high-carbon martensite steel, *Sci. Rep.*, 7(2017), art. No. 6596.
[62] Y.H. Gao, S.Z. Liu, X.B. Hu, *et al*., A novel low cost 2000 MPa grade ultra-high strength steel with balanced strength and toughness, *Mater. Sci. Eng. A*, 759(2019), p. 298.
[63] M.S. Baek, Y.K. Kim, T.W. Park, J. Ham, and K.A. Lee, Hot-rolling and a subsequent direct-quenching process enable super-

ior high-cycle fatigue resistance in ultra-high strength low alloy steels, *Materials*, 13(2020), No. 20, art. No. 4651.
[64] Y.J. Wang, J.J. Sun, T. Jiang, Y. Sun, S.W. Guo, and Y.N. Liu, A low-alloy high-carbon martensite steel with 2.6 GPa tensile strength and good ductility, *Acta Mater.*, 158(2018), p. 247.
[65] J.M. Zhu, H.H. Wu, Y. Wu, *et al*., Influence of Ni_4Ti_3 precipitation on martensitic transformations in NiTi shape memory alloy: R phase transformation, *Acta Mater.*, 207(2021), art. No. 116665.
[66] Z.J. Gao, S.Z. Wang, H.H. Wu, J.Y. Li, and X.P. Mao, Understanding the mismatch strain and orientation of nanoscale second phase on the superelasticity of zirconia, *Compos. Commun.*, 22(2020), art. No. 100521.
[67] M. Kapoor, D. Isheim, S. Vaynman, M.E. Fine, and Y.W. Chung, Effects of increased alloying element content on NiAl-type precipitate formation, loading rate sensitivity, and ductility of Cu- and NiAl-precipitation-strengthened ferritic steels, *Acta Mater.*, 104(2016), p. 166.
[68] B.C. Zhou, T. Yang, G. Zhou, H. Wang, J.H. Luan, and Z.B. Jiao, Mechanisms for suppressing discontinuous precipitation and improving mechanical properties of NiAl-strengthened steels through nanoscale Cu partitioning, *Acta Mater.*, 205(2021), art. No. 116561.
[69] W.W. Sun, R.K.W. Marceau, M.J. Styles, D. Barbier, and C.R. Hutchinson, G phase precipitation and strengthening in ultra-high strength ferritic steels: Towards lean 'maraging' metallurgy, *Acta Mater.*, 130(2017), p. 28.
[70] J. Millán, S. Sandlöbes, A. Al-Zubi, *et al*., Designing Heusler nanoprecipitates by elastic misfit stabilization in Fe–Mn maraging steels, *Acta Mater.*, 76(2014), p. 94.
[71] M. Kapoor, D. Isheim, G. Ghosh, S. Vaynman, M.E. Fine, and Y.W. Chung, Aging characteristics and mechanical properties of 1600MPa body-centered cubic Cu and B2-NiAl precipitation-strengthened ferritic steel, *Acta Mater.*, 73(2014), p. 56.
[72] Y. Li, W. Li, W.Q. Liu, *et al*., The austenite reversion and co-precipitation behavior of an ultra-low carbon medium manganese quenching–partitioning–tempering steel, *Acta Mater.*, 146(2018), p. 126.
[73] Z.B. Jiao, J.H. Luan, M.K. Miller, and C.T. Liu, Precipitation mechanism and mechanical properties of an ultra-high strength steel hardened by nanoscale NiAl and Cu particles, *Acta Mater.*, 97(2015), p. 58.
[74] X.C. Yang, X.J. Di, Q.Y. Duan, W. Fu, L.Z. Ba, and C.N. Li, Effect of precipitation evolution of NiAl and Cu nanoparticles on strengthening mechanism of low carbon ultra-high strength seamless tube steel, *Mater. Sci. Eng. A*, 872(2023), art. No. 144939.
[75] W. Sha, A. Ye, S. Malinov, and E.A. Wilson, Microstructure and mechanical properties of low nickel maraging steel, *Mater. Sci. Eng. A*, 536(2012), p. 129.
[76] F. Qian, J. Sharp, and W.M. Rainforth, Microstructural evolution of Mn-based maraging steels and their influences on mechanical properties, *Mater. Sci. Eng. A*, 674(2016), p. 286.
[77] A. Behravan, A. Zarei-Hanzaki, S.M. Fatemi, H.F.G. De Abreu, and M. Masoumi, The effect of aging temperature on microstructure and tensile properties of a novel designed Fe–12Mn–3Ni maraging-TRIP steel, *Steel Res. Int.*, 90(2019), No. 2, art. No. 1800282.
[78] K. Li, L. Wei, B. Yu, and R.D.K. Misra, Reverted austenite with distinct characteristics in a new cobalt-free low lattice misfit precipitate-bearing 19Ni3Mo1.5Ti maraging steel, *Mater. Lett.*, 257(2019), art. No. 126692.
[79] F. Qian and W.M. Rainforth, The formation mechanism of reverted austenite in Mn-based maraging steels, *J. Mater. Sci.*, 54(2019), No. 8, p. 6624.
[80] E.I. Galindo-Nava, W.M. Rainforth, and P.E.J. Rivera-Díaz-del-Castillo, Predicting microstructure and strength of maraging steels: Elemental optimisation, *Acta Mater.*, 117(2016), p. 270.
[81] H.L. Zhang, M.Y. Sun, D.P. Ma, *et al*., Effect of aging temperature on the heterogeneous microstructure and mechanical properties of a 12Cr–10Ni–Mo–Ti maraging steel for cryogenic applications, *J. Mater. Sci.*, 56(2021), No. 19, p. 11469.
[82] S. Bodziak, K.S. Al-Rubaie, L.D. Valentina, *et al*., Precipitation in 300 grade maraging steel built by selective laser melting: Aging at 510 °C for 2 h, *Mater. Charact.*, 151(2019), p. 73.
[83] E.A. Jägle, P.P. Choi, J.V. Humbeeck, and D. Raabe, Precipitation and austenite reversion behavior of a maraging steel produced by selective laser melting, *J. Mater. Res.*, 29(2014), No. 17, p. 2072.
[84] V.K. Vasudevan, S.J. Kim, and C.M. Wayman, Precipitation reactions and strengthening behavior in 18 Wt Pct nickel maraging steels, *Metall. Trans. A*, 21(1990), No. 10, p. 2655.
[85] T.Z. Xu, S. Zhang, Y. Du, *et al*., Development and characterization of a novel maraging steel fabricated by laser additive manufacturing, *Mater. Sci. Eng. A*, 891(2024), art. No. 145975.
[86] Y. Du, T.Z. Xu, S. Zhang, *et al*., Effect of aging treatment on the microstructure and tribological properties of a new maraging steel manufactured by laser directed energy deposition, *Mater. Charact.*, 209(2024), art. No. 113767.
[87] J.M. Pardal, S.S.M. Tavares, V.F. Terra, M.R.D. Silva, and D.R.D. Santos, Modeling of precipitation hardening during the aging and overaging of 18Ni–Co–Mo–Ti maraging 300 steel, *J. Alloys Compd.*, 393(2005), No. 1-2, p. 109.
[88] J.J.M. da Silva, I.F. de Vasconcelos, F.I.S. da Silva, T.S. Ribeiro, and H.F.G. de Abreu, An atomic redistribution study of the 440°C ageing kinetics in maraging-300 steel, *Mater. Res.*, 22(2019), No. 1, art. No. e20180230.
[89] T.Z. Xu, S. Zhang, L. Wang, *et al*., Influence of scanning speed on the microstructure, nanoindentation characteristics and tribological behavior of novel maraging steel coatings by laser cladding, *Mater. Charact.*, 205(2023), art. No. 113335.
[90] M. El-Meligy, T. El-Bitar, and S. Ebied, Creation of fine lath martensite combined with nano needle like structured carbides in ultra high strength (UHS) military Steel, *J. Ultrafine Grained Nanostruct. Mater.*, 56(2023), No. 2, p. 173.
[91] M.J. Yang, C. Huang, Z.F. Yao, *et al*., Development of a high-strength Fe–12Mn maraging steel *via* designing lath interfacial and intragranular nanostructures, *Mater. Sci. Eng. A*, 886(2023), art. No. 145280.
[92] Z.Y. Zhang, F. Chai, X.B. Luo, G. Chen, C.F. Yang, and H. Su, The strengthening mechanism of Cu bearing high strength steel as-quenched and tempered and Cu precipitation behavior in steel, *Acta Metall. Sin.*, 55(2019), No. 6, p. 783.
[93] T. Gladman, Precipitation hardening in metals, *Mater. Sci. Technol.*, 15(1999), No. 1, p. 30.
[94] L. Proville and B. Bakó, Dislocation depinning from ordered nanophases in a model fcc crystal: From cutting mechanism to Orowan looping, *Acta Mater.*, 58(2010), No. 17, p. 5565.
[95] Q.H. Fang, L. Li, J. Li, *et al*., A statistical theory of probability-dependent precipitation strengthening in metals and alloys, *J. Mech. Phys. Solids*, 122(2019), p. 177.
[96] P. Han, Z.P. Liu, Z.J. Xie, *et al*., Influence of band microstructure on carbide precipitation behavior and toughness of 1 GPa-grade ultra-heavy gauge low-alloy steel, *Int. J. Miner. Metall. Mater.*, 30(2023), No. 7, p. 1329.
[97] Z.J. Xie, Y.P. Fang, G. Han, H. Guo, R.D.K. Misra, and C.J. Shang, Structure–property relationship in a 960MPa grade ultrahigh strength low carbon niobium–vanadium microalloyed steel: The significance of high frequency induction tempering, *Mater. Sci. Eng. A*, 618(2014), p. 112.